iScience

CellPress
OPEN ACCESS

Article

In vivo library screening identifies the metabolic enzyme aldolase A as a promoter of metastatic lung colonization

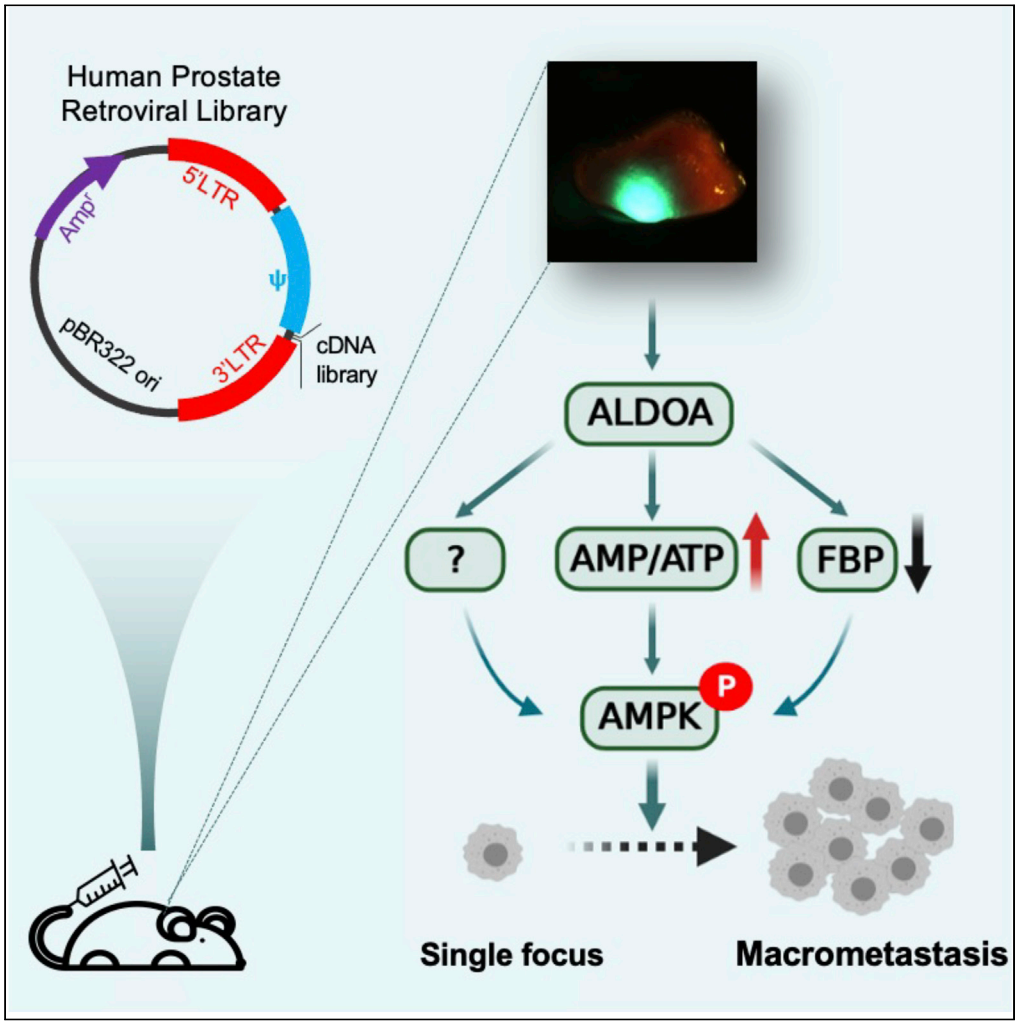

Zhenbo Tu, Shengqi Hou, Yurong Zheng, Maerjianghan Abuduli, Tamer Onder, Andrew M. Intlekofer, Antoine E. Karnoub

akarnoub@bidmc.harvard.edu

Highlights

Gain-of-function cDNA screen identifies several potential metastatic genes

Aldolase A promotes metastatic lung colonization

Aldolase A regulates AMPK-dependent malignancy traits in cancer cells

Aldolase A is a prognostic biomarker of cancer progression

Tu et al., iScience *24*, 102425
May 21, 2021
https://doi.org/10.1016/j.isci.2021.102425

iScience

CellPress
OPEN ACCESS

Article

In vivo library screening identifies the metabolic enzyme aldolase A as a promoter of metastatic lung colonization

Zhenbo Tu,[1] Shengqi Hou,[2] Yurong Zheng,[1] Maerjianghan Abuduli,[1] Tamer Onder,[3] Andrew M. Intlekofer,[2] and Antoine E. Karnoub[1,4,5,6,*]

SUMMARY

Elucidations of the factors that promote the growth of disseminated tumor cells (DTCs) into life-threatening lesions stand to provide much needed prognostic and therapeutic targets of translational utility for patients with metastatic cancer. To identify such regulators, we conducted gain-of-function cDNA library screening to discover genes that foster prostate cancer cell colonization of mouse lungs as an experimental model. Our efforts identified the metabolic enzyme aldolase A (ALDOA) as a driver of cancer cell motility, anchorage-independent growth, and metastatic colonization, and as a prognosticator of adverse patient outcome across many malignancies, including prostate, breast, pancreatic, and liver cancers. Metabolomics coupled with biochemical and functional analyses revealed that ALDOA triggered the activation of adenosine-5′-monophosphate (AMP)-activated protein kinase (AMPK), which we demonstrate played essential promalignant activities in ALDOA-expressing cells. Collectively, these findings unveiled vivo approaches to identify metastatic colonization regulators and uncovered previously undescribed roles for ALDOA-AMPK pathway in tumor progression.

INTRODUCTION

Cancer continues to represent the second leading cause of death in the United States, with more than 600,000 fatalities projected for 2020 alone (Siegel et al., 2020). Although steady improvements in early detection, diagnosis, and clinical management have improved the survival odds for many patients with cancer, those who exhibit metastatic disease still face limited therapeutic options with increased morbidity and mortality. As >90% of cancer deaths occur because of metastasis, detailed identification and characterization of critical pathways that drive malignant progression are essential to the development of effective diagnostics and treatments for advanced disease (Steeg, 2016).

The classical view of metastasis development encompasses a cascade of sequential events that metastasizing cancer cells within primary tumors effectuate, which include intravasation into circulation, survival during transit, dissemination into the parenchyma of secondary sites through extravasation, and finally, colonization of target organs (Spano et al., 2012). Of all these steps, metastatic colonization of secondary tissues is considered to be the most difficult and least efficient process. Indeed, faced with the constraints of the target tissue microenvironment, the overwhelming majority of disseminated tumor cells (DTCs) either undergoes apoptotic cell death or maintains a period of cell-cycle arrest or dormancy that could last for years (Kienast et al., 2010; Vanharanta and Massague, 2013). While research advances have provided critical insights into the molecular and cellular frameworks underlying cancer cell spread, the intrinsic and extrinsic factors that regulate the time frame and the manner through which some DTCs grow into life-threatening lesions remains incompletely understood (Giancotti, 2013; Zhang et al., 2019). Research into this area is therefore of increased importance and stands to provide therapeutic targets of potential translational utility in patient management.

In the present study, we aimed at identifying intrinsic genetic elements that foster cancer cell metastatic colonization of secondary tissues using a gain-of-function (GOF) cDNA library screening approach. GOF cDNA screening has been successfully used *in vitro* to discover genes relevant to multiple phenotypes of relevance to cancer, such as regulators of apoptosis (Martin et al., 2004; Yamaji et al., 2010), senescence

[1]Department of Pathology and Cancer Center, Beth Israel Deaconess Medical Center, Harvard Medical School, Boston, MA 02215, USA

[2]Human Oncology and Pathogenesis Program and Department of Medicine, Memorial Sloan Kettering Cancer Center, New York 10065, USA

[3]Department of Molecular Biology and Genetics, School of Medicine, Koç University, Istanbul 34450, Turkey

[4]Harvard Stem Cell Institute, Cambridge, MA 02138, USA

[5]Broad Institute of MIT and Harvard, Cambridge, MA 02142, USA

[6]Lead contact

*Correspondence: akarnoub@bidmc.harvard.edu

https://doi.org/10.1016/j.isci.2021.102425

(Brummelkamp et al., 2002), or cell growth (He et al., 2010), and we decided to use it *in vivo* to uncover genetic drivers of cancer colonization of the lung as a metastatic tissue. Our efforts led to the identification of the metabolic enzyme aldolase A (ALDOA) as a driver of prostate cancer cell motility, anchorage independent growth, and metastasis, and as a clinically relevant prognostic biomarker of cancer patient survival across many tumor types. Mechanistic studies indicated the dependency of ALDOA promalignant activities on the energy sensor adenosine-5′-monophosphate (AMP)-activated protein kinase (AMPK), revealing previously unappreciated roles for this pathway in metastasis.

RESULTS

cDNA-library-based screening for metastatic lung colonization factors

Cancer cells that seed secondary sites exhibit wide heterogeneity in their propensities to grow in their new microenvironments, with some remaining as micrometastases while others forming more pronounced macrometastatic growths (Giancotti, 2013). To identify cell-intrinsic genetic events that promote cancer cell metastatic colonization, we first sought to identify cancer cell lines that predominantly form micrometastases once introduced into the systemic circulation of recipient mice. We focused on the lung as a secondary metastasis tissue because lung metastasis is observed in many advanced human carcinomas, such as breast, colorectal, skin, or prostate cancers (Obenauf and Massague, 2015), and because of the experimental ease of metastatic colony visualization in, and isolation from, excised lung tissues.

For these purposes, we stably expressed GFP in target cancer cells, which included murine mammary carcinoma cell lines 168FARN, 67NR, and 4T07, human breast cancer cells MCF7/Ras, MDA-MB-231, and HMLER, human colon cancer cells SW620, and human prostate cancer cell line DU145, and injected 150 $x10^3$ labeled cells into the systemic circulation of recipient NOD/SCID mice via the retro-orbital route. Fluorescence-microscopy-based examination of lungs excised 18 days later revealed wide variations in the colonization abilities of tested cells (Figure S1). Indeed, while HMLER cells, used here as a positive control, and 67NR cells predominantly formed large (>1 mm in diameter) colonies at the mean rates of ~50 macrometastases per lung, other cell lines, such as MDA-MB-231, gave rise to both micrometastases and macrometastases, with visible >1 mm-clusters at the rate of ~40 macrometastases per lung. Of note were SW620 and DU145 cells, which tended to form much fewer macrometastases than the aforementioned cell lines. However, in contrast to SW620, which did not give rise to discernable micrometastases, DU145 cells predominantly formed singletons with occasional formation of >1 mm clusters. For these reasons, we chose DU145 as the cell of choice for further analysis.

pLIB-based retroviral cDNA libraries have been successfully used to uncover genetic elements involved in regulating a wide array of phenotypes, including cellular senescence (Brummelkamp et al., 2002), growth (Berns et al., 2000), and metastasis (Martin et al., 2004), and we chose to use pLIB prostate library cDNA derived from normal prostate tissue for our screen. The prostate cDNA library (containing >$8.0x10^6$ clones, with a cDNA size range of 0.5–5.0 kb and with average size cDNA length of 1.6 kb) was transfected into HEK293T cells, and recovered viral particles were transduced at low titers into GFP-DU145 cells. (MOI was 0.2 determined using manufacturer supplied pLAPSN as a control to minimize more than 1 virus per cell). Empty-pBabe-carrying control particles transduced in parallel into GFP-DU145 cells served as library controls. Infected control and pLIB-GFP-DU145 cells were harvested 48 h later, and injected intravenously via tail-veins of recipient male NOD/SCID mice at the rate of $150x10^3$ cells per animal (Figure S2A). As expected, microscopic examination of control lungs 18 days later revealed little, if any, macrocolonies, with several micrometastases identified (Figure S2B). In contrast, pLIB-GFP-DU145-injected mice exhibited multiple (>12–15) visible growths that were either imbedded deep in the lungs or surface-exposed (Figure S2B). These results suggested that cDNA inserts derived from the pLIB library enabled the growth of DU145 cells as macrocolonies in the mouse lungs.

To identify library-derived cDNA inserts present in the GFP colonies, we surgically excised the individual growths and subjected them to genomic PCR using primers specific to the 5′ and 3′ linker sequences imbedded into each library cDNA. Reactions were resolved by electrophoresis and isolated amplicons were sequenced for identification. Of the full sequences recovered from separate colonies were those for ceroid lipofuscinosis neuronal 8 (CLN8), NADH:ubiquinone oxidoreductase core subunit S2, ribosomal protein S20, Rab GTPase-activating protein 1, kallikrein-related peptidase 3 (KLK3), CCR4-NOT Transcription Complex Subunit 2, laminin receptor (67LR) (also known as RPSA), and ALDOA (Figure S2C). The presence of factors with putative metastasis-promoting functions on this list, such as RPSA or 67LR (Fulop and Larbi,

2002), suggested that our screen has led to the identification of genes of important regulatory roles in metastatic colonization.

ALDOA promotes metastatic colonization

We specifically became interested in ALDOA. Indeed, while other full-length cDNAs were identified once from individual growths, ALDOA was recurrently identified from 3 separate metastatic growths. Furthermore, ALDOA encodes an enzyme that catalyzes the conversion of fructose 1,6-bisphosphate (F-1,6-BP or FBP) to glyceraldehyde 3-phosphate (G-3P) and dihydroxyacetone phosphate, a key gate-keeping metabolic step in glycolysis and one that can ostensibly regulate the ability of cancer cells to grow or go into quiescence when seeded in secondary tissues. In addition, although prior studies have associated elevated ALDOA expression with cancer progression or adverse patient survival in contexts of lung cancer (Du et al., 2014; Lin et al., 2011), gastric cancer (Morisaki et al., 2014), or osteosarcoma (Chen et al., 2014; Long et al., 2014), potential regulatory roles for ALDOA in prostate cancer cell metastatic colonization of secondary tissues have not been reported. These considerations, together with the predominant expression of ALDOA versus its isozymes ALDOB or ALDOC in several prostate cancer cells (namely, DU145, PC3, LNCAP, C4-2, and RV-1; Figure 1A), prompted us to determine if ALDOA was sufficient, on its own, in promoting the acquisition of malignant traits by DU145 cells, specifically traits conducive to lung macrometastasis formation.

ALDOA sequence was tagged with a hemagglutinin epitope at the NH_2-terminal, cloned into pLenti-CMV, and stably expressed in DU145-GFP cells by puromycin selection. After confirmation of mRNA and protein overexpression (Figures 1B and 1C), along with specific enzyme activation (Figure 1D), we proceeded to characterize the phenotypes of ALDOA-DU145 cells. Here, we found that ALDOA overexpression did not alter the growth properties of adherent DU145 cells (Figure S3A) and had no measurable effect on cell cycle distribution of the cultures (Figure S3B). Furthermore, exogenous ALDOA did not affect the ability of DU145 cells to withstand suspension-induced cell death (anoikis; Figure S3C). Interestingly, however, ALDOA enhanced cellular migration in Boyden chamber setups by ~2.5 times (Figure 1E), promoted cellular invasion through matrigel by ~50% (Figure 1F), and enhanced the ability of cancer cells to grow in anchorage-independence by ~5 times (Figure 1G). Most importantly, ALDOA-DU145 cells seeded into the lungs of male NOD/SCID mice by intravenous tail-vein injections formed macrocolonies in the mouse lungs at >3 times the rates of their control counterparts (average of 3.17 and 14.4 clusters for control and ALDOA-DU145 cells, respectively; Figure 1H). These results indicated that ALDOA indeed promoted various aspects of cancer cell malignancy and that it enabled seeded cancer cells to colonize secondary sites.

Critical role for AMPK in ALDOA-induced malignancy

The aforementioned results highlighted the importance of intrinsic ALDOA activities to metastasis formation, and we set out to determine its molecular mechanism of action in these contexts. To this end, we adopted several concerted approaches. First, we used STRING analysis to identify the protein association network of ALDOA, which included 10 proteins of established metabolic functions, such as triosephosphate isomerase, transketolase, or phosphofructokinase, platelet (Figure 2A). We then used these 10 markers to conduct KEGG pathway enrichment analysis, which pointed to a number of associated pathways, such as glycolysis/gluconeogenesis, pentose phosphate pathway, RNA degradation, and HIF-1 signaling pathway (Figure 2B) as possibly regulated by ALDOA. In addition, because ALDOA exerted prometastatic functions, we proceeded to determine the ALDOA-correlated gene sets and pathways present within clinical prostate cancer metastasis, focusing specifically on the two largest metastatic prostate cancer data sets in The Cancer Genome Atlas: Metastatic Prostate Adenocarcinoma and Metastatic Prostate Cancer, which included 2,758 and 3,435 genes, respectively. DAVID-based gene enrichment analysis of the 1,599 genes common to these two data sets led to the identification of a number of pathways, for example, insulin signaling, carbon metabolism, HIF-1 signaling, or biosynthesis of amino acids, largely emphasizing the role of metabolism in prostate cancer progression (Figure 2C). To confirm/validate these findings in our own system, we thirdly conducted liquid chromatography–tandem mass spectrometry-based metabolomic analyses of our HA-ALDOA-DU145 cells as compared with their controls. These experiments indicated 37 products that were significantly upregulated (>1-fold, $p < 0.05$) in the HA-ALDOA-DU145 cells (of ~122 screened metabolites; Figure S4A), which, when passed through MetaboAnalyst, revealed accentuation of pathways such as the citric acid cycle and the Warburg effect by ALDOA (Figure 2D). Only twelve metabolic products were significantly decreased, which included,

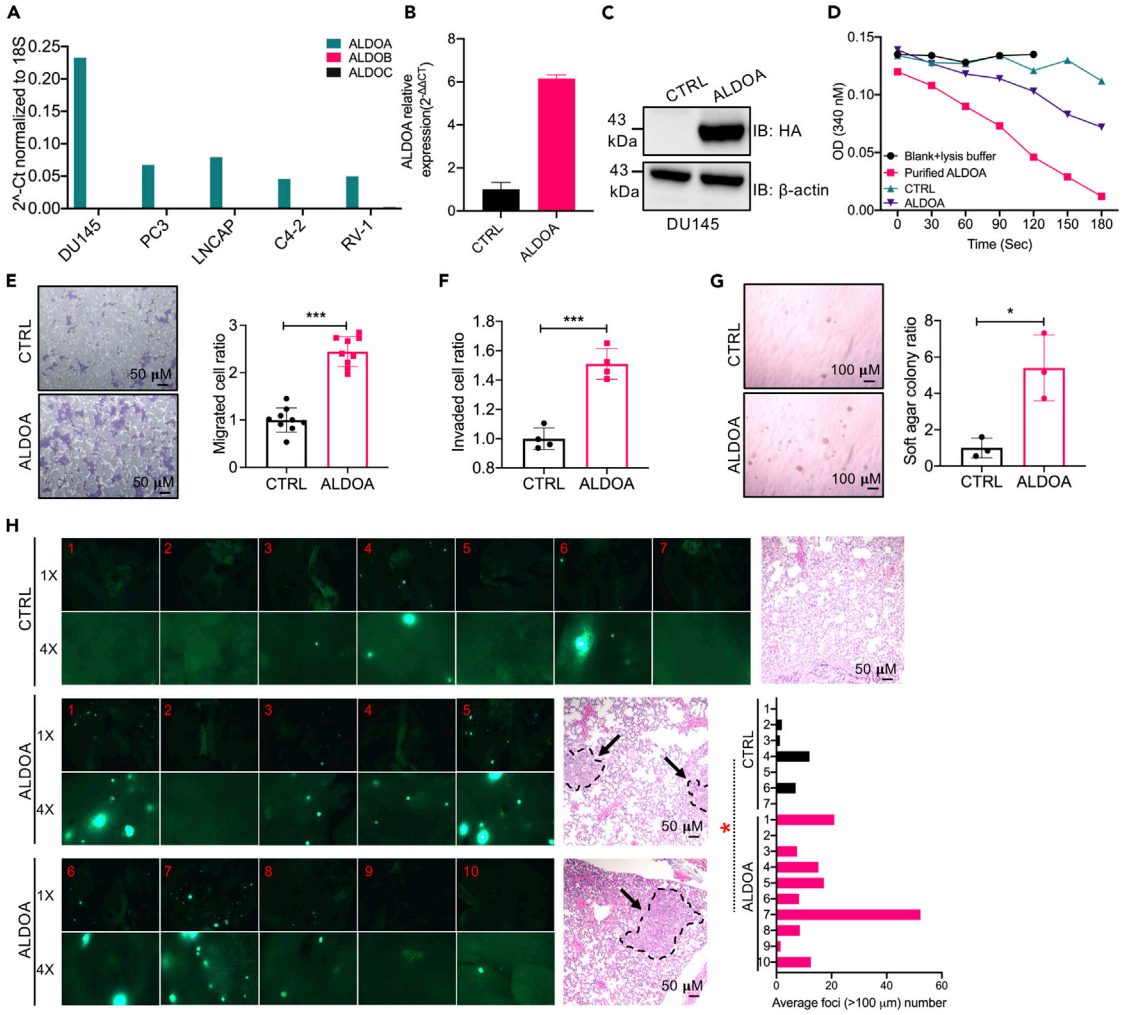

Figure 1. ALDOA promotes cell migration, anchorage-independent growth, and macrometastasis formation

(A) Endogenous expression levels of ALDOA, ALDOB, and ALDOC in DU145, PC3, LNCAP, C4-2, and RV-1 cells by QRT-PCR. Values were normalized to 18S (representative mean of n = 3 in triplicates each).

(B and C) Expression levels (mean ± SD) of HA-ALDOA in the indicated DU145 cells determined by QRT-PCR (normalized to 18S; left) and Western blotting (normalized to actin; right); n > 3 in triplicates each.

(D) ALDOA enzymatic activity in DU145 cells stably expressing HA-ALDOA (ALDOA) and controls (CTRL), with purified Aldolase A used as a positive control. Representative assay is shown from n > 4 in duplicates each.

(E) Representative images (left) and quantification (right) of migration analyses of control versus HA-ALDOA-overexpressing DU145 cells. Data are displayed as mean ± SD of n = 9 in triplicates each. ***p < 0.001, unpaired t test. Scale bars indicate 50 μm.

(F) Quantification of invasion analyses of control versus HA-ALDOA-overexpressing DU145 cells. Data are displayed as mean ± SD of n = 4 in triplicates each. ***p < 0.001, unpaired t test.

(G) Representative images (left) and quantification (right; mean ± SD of n = 3 in triplicates each) of soft-agar assays performed on controls and HA-ALDOA-overexpressing DU145 cells. *p < 0.05, unpaired t test. Scale bars indicate 100 μm.

(H) Representative pictures of GFP-fluorescence and H and E staining in mouse lungs 18 days after control (CTRL) or HA-ALDOA-overexpressing DU145 cells expressing GFP were injected ($150x10^3$/mouse) into the tail-vein in male NOD/SCID mice. Data represent mean ± SD. *p < 0.05, unpaired t test. Scale bars indicate 50μm.

See also Figures S1–S3.

for example, ribose-5-phosphate or oxidized glutathione, suggestive of deregulations in the pentose phosphate pathway (PPP) and oxidative stress, respectively (Figure S4B).

Of particular interest from all these approaches was AMPK, which we hypothesized that it played important roles in ALDOA-mediated functions. Indeed, the AMPK pathway was recurrently flagged as a significantly

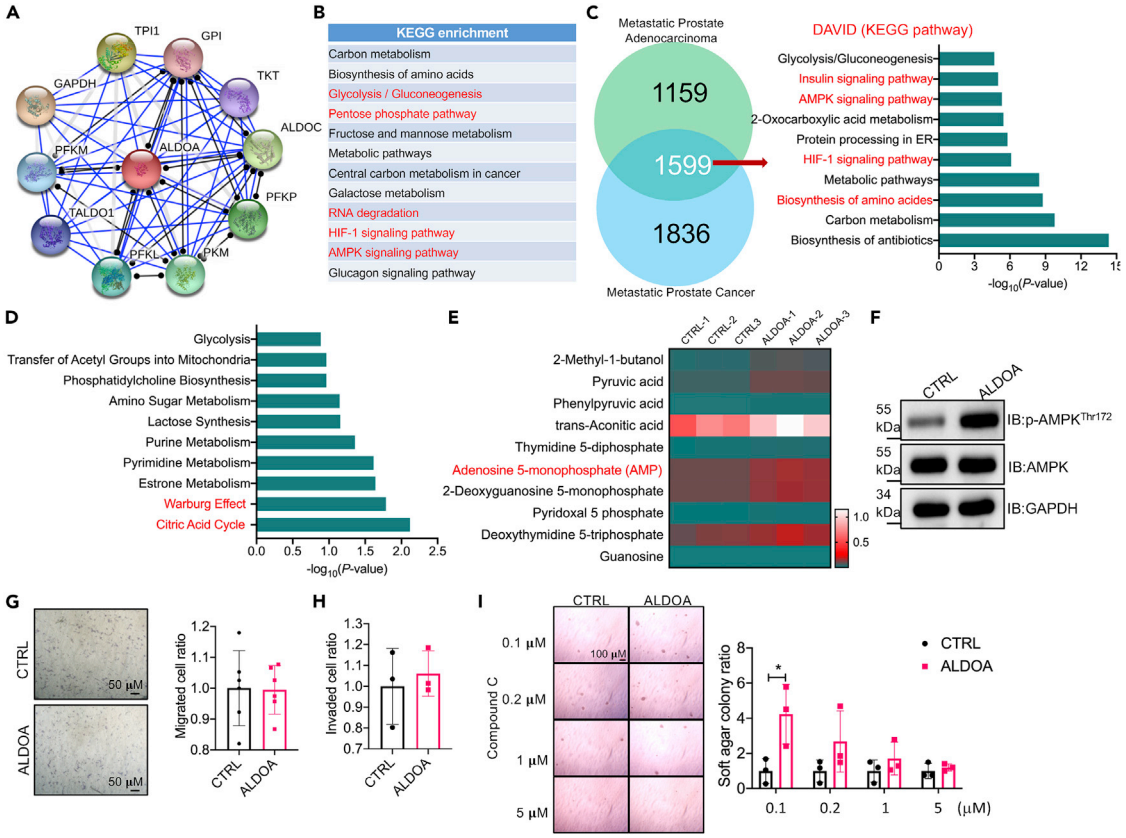

Figure 2. ALDOA activates AMPK

(A) Visualization of ALDOA network from STRING.

(B) KEGG enrichment of ALDOA network components from STRING.

(C) Left: Venn diagram of the common genes positively correlated with ALDOA ($r > 0.25$, $p < 0.05$) from Metastatic Prostate Adenocarcinoma (SU2C/PCF Dream Team) and Metastatic Prostate Cancer (SU2C/PCF Dream Team) data. Right: KEGG pathway analysis of the 1599 common genes using DAVID.

(D) KEGG analysis of upregulated metabolic products (derived from LC/MS) in DU145 cells stably expressing HA-ALDOA analyzed via MetaboAnalyst.

(E) Heat map generated from standard LC/MS quantitative analyses reflects the top 10 upregulated metabolic products showing differential abundance levels between DU145 stably expressing HA-ALDOA cells and control cells. Analysis is carried out as two-way *t* test with a threshold of $p < 0.05$. Samples are arranged in column while the metabolites are arranged in rows. (color coding: red to light red shades indicate increased expression.)

(F) Representative ($n > 3$) Western blots of phospho-AMPK and AMPK in DU145 cells stably expressing HA-ALDOA and controls. GAPDH was used as a loading control.

(G) Representative images (left) and quantification (right) of migration analyses of control versus HA-ALDOA-overexpressing DU145 cells treated with Compound C (5μM). Data are displayed as mean ± SD of $n = 6$ in triplicates each. Scale bars indicate 50 μm.

(H) Quantification of invasion analyses of control versus HA-ALDOA-overexpressing DU145 cells treated with Compound C (5 μM). Data are displayed as mean ± SD of $n = 3$ in triplicates each.

(I) Representative images (left) and quantification (right) of soft-agar analyses of control versus HA-ALDOA-overexpressing DU145 cells treated with the indicated doses of Compound C twice weekly. Data are displayed as mean ± SD of $n = 3$ in triplicates each. Scale bars indicate 100 μm. *$p < 0.05$, unpaired t test.

See also Figures S4–S6.

enriched pathway in both our STRING/KEGG analyses and our TCGA-based pathway enrichment classifications (Figures 2B and 2C). In addition, AMPK is a master regulator of glycolysis, TCA cycle, Warburg effect, PPP pathway, amino acid biosynthesis, and HIF-1 signaling, all of which were flagged as significantly upregulated by HA-ALDOA using LC/MS (Figure 2D). Furthermore, we noticed that AMP, the building block for the generation of adenosine diphosphate and adenosine-5′-triphosphate (ADP and ATP, respectively) and an allosteric activator of AMPK (20, 21), was the sixth most induced metabolite in HA-ALDOA-DU145 cells with an accumulation of 1.5-fold over controls (Figures S4A and 2E). Supporting our assumption was also the finding that the ratio of AMP over ATP, considered a major rheostat for AMPK activation (20, 21), was in fact increased by ~35% ($p < 0.05$) in HA-ALDOA-expressing cells (Figure S5). Finally, AMPK is an energy/stress sensor with demonstrated roles in regulating key metabolic pathways, such as citric acid

cycle or purine metabolism (Garcia and Shaw, 2017; Steinberg and Carling, 2019), all of which were also identified as being enriched in our pathway analyses (Figure 2D).

In line with these observations, we found that exogenous ALDOA significantly induced the phosphorylation of AMPK at Thr172 (Figure 2F), an activation loop modification tightly linked to AMPK activation (Garcia and Shaw, 2017; Steinberg and Carling, 2019). This induction appeared to depend on the metabolic activity of ALDOA because the active site mutant ALDOA^{D34A} was unable to stimulate AMPK^{T172} phosphorylation (Figure S6A). Importantly, ALDOA^{D34A} was also defective in promoting cellular migration (Figure S6B), and inhibition of AMPK using Compound C severely inhibited ALDOA-triggered migration (Figure 2G), invasion (Figure 2H), and anchorage-independent growth (Figure 2I). Together, these observations highlighted tight linkages between ALDOA activation and AMPK^{T172} induction and underscored the essentiality of AMPK to ALDOA promalignant functions.

ALDOA is a clinical prognosticator of cancer progression and patient outcome

To examine the relevance of ALDOA to disease progression in the clinic, we queried its expression in a series of publicly available gene set databases. First, we found the mean expression value of ALDOA to be > 2 fold higher in patients with prostate cancer compared with normal controls (GENT2; Figure 3A). In addition, the levels of ALDOA were significantly higher in primary metastatic prostate cancers when compared with nonmetastatic counterparts in three different cohorts (GSE3325, GSE6919, and GSE6099; Figures 3B–3D). Furthermore, ALDOA was enriched in prostate cancer metastases, especially from bone (GSE77930; Figure 3E), a frequent metastatic site in prostate cancer (DiNatale and Fatatis, 2019), further underscoring the tight correlation of ALDOA with clinical disease progression. Importantly, area-under-the-curve (AUC) analyses on the same aforementioned cohorts revealed significant diagnostic accuracy for ALDOA in GSE3325 with AUC = 1.0 (95% confidence interval [CI]: 1.0–1.0; P = 0.003) (Figure 3F), in GSE6919 with AUC = 0.91 (95% CI: 0.853–0.967; P = 0.000) (Figure 3G), in GSE6099 with AUC = 0.781 (95% CI: 0.649–0.913; P = 0.001) (Figure 3H), and in GSE77930 with AUC = 0.858 (95% CI: 0.764–0.953; P = 0.000) (Figure 3I). Similarly, Kaplan-Meier (KM)-based analyses associated elevated ALDOA levels with diminished disease-free survival odds in a cohort of ~500 patients with prostate cancer (Figure 3J), altogether emphasizing the role of ALDOA as a clinically relevant prognosticator in prostate cancer.

Although TCGA-based analyses indicated particular enrichment of ALDOA in metastatic prostate cancer or neuroendocrine prostate cancer, other types of tumors also exhibited amplification of ALDOA, especially breast cancers (Figure 4A). Indeed, similarly to what we have seen with DU145 cells, overexpression of HA-ALDOA in breast cancer cell line MDA-MB-231 cells (Figure 4B) augmented their migratory (Figure 4C) and invasive (Figure 4D) behavior and almost doubled their ability to grow in anchorage independence (Figure 4E). In parallelism to what we observed in DU145 cells, WT ALDOA, but not ALDOA^{D34A}, promoted AMPK phosphorylation in MDA-MB-231 cells (Figure S6C), and ALDOA^{D34A}-expressing MDA-MB-231 cells were not more migratory than controls (Figure S6D). In addition, Compound C treatment abolished ALDOA-induced migration (Figure 4C) and invasion (Figure 4D) in this model, again corroborating our observations in DU145 cells.

Consistent with the aforementioned results, higher ALDOA levels were seen in primary breast tumors than in normal tissues (Figure 4F), which also associated with metastatic progression (Figure 4G). Of interest, KM analyses of >2,600 patients with breast cancer indicated a strong association of high ALDOA with poor patient survival (Figure 4H), particularly in the basal subtype (Figure 4I) and in patients with identified lymph node metastases (Figure 4J). Along the same lines, we found similar trends when examining ALDOA in additional tumor types. Here, ALDOA levels were higher in cancer versus normal tissues and were predictive of patient survival and/or disease progression in pancreatic (Figures 4K and 4L), lung (Figures 4M and 4N), and liver (Figures 4O–4Q) cancers. Collectively, these results suggested the generalized functions of ALDOA as a promalignancy biomarker of disease progression in settings beyond prostate cancer.

DISCUSSION

Cancer cell colonization of secondary tissues represents the most enigmatic bottleneck step in metastasis (Vanharanta and Massague, 2013). Indeed, the intrinsic and extrinsic factors that regulate if and when seeded cancer cells engender life-threatening growths remain largely uncharacterized (Giancotti, 2013). Therefore, elucidation of the molecular mechanisms underlying colonization is of paramount importance

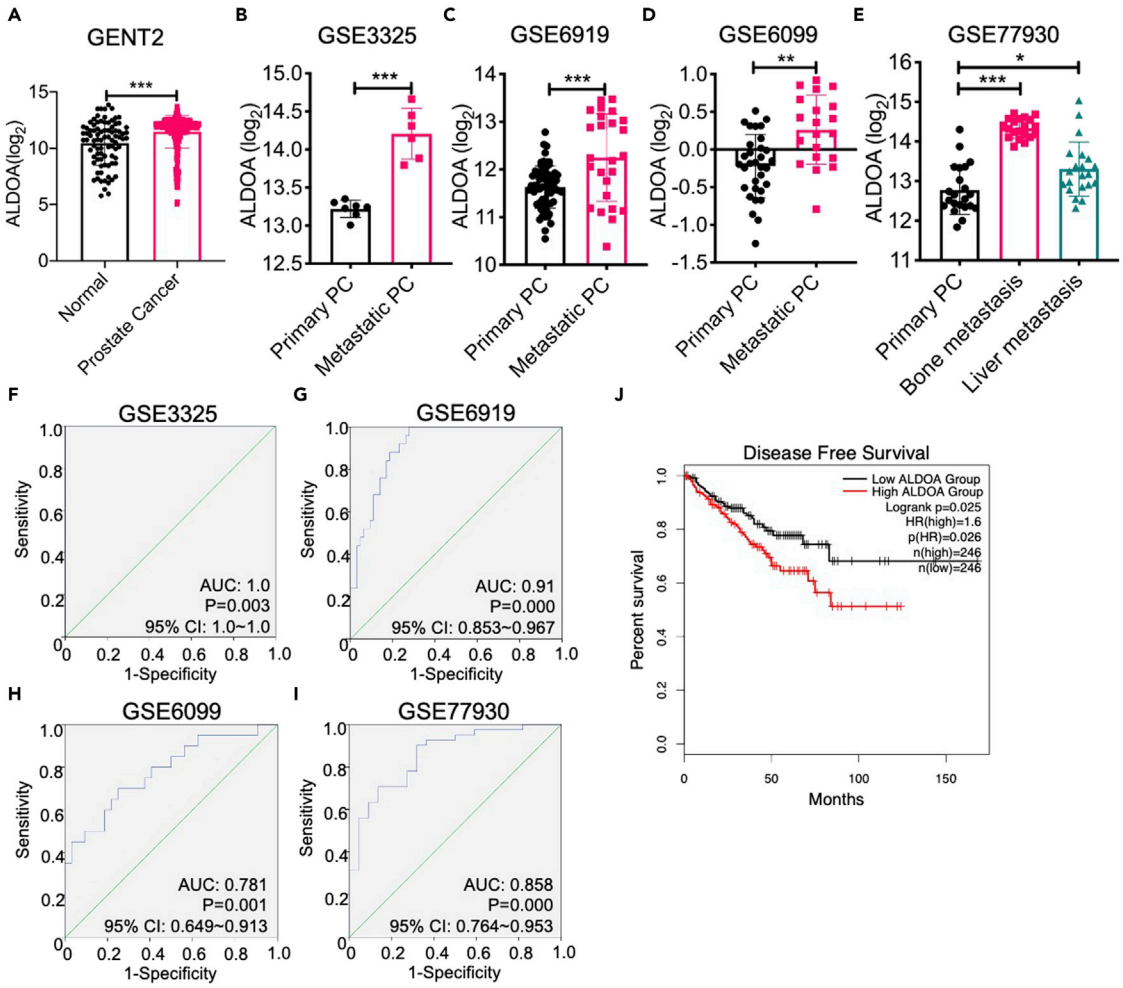

Figure 3. ALDOA associates with advanced prostate cancer

(A) ALDOA levels in normal patients (n = 86) and patients with prostate cancer (n = 323) from GENT2. Data represent the mean ± SD. ***p < 0.001, unpaired t test.

(B) ALDOA levels (Probe: 200966_x_at and 214687_x_at) in primary (n = 7) and metastatic prostate cancer (n = 6) patients in GSE3325. Data represent the mean ± SD. ***p < 0.001, unpaired t test.

(C) ALDOA levels (Probe: 32336_at) in primary (n = 65) and metastatic prostate cancer (n = 25) patients in GSE6919. Data represent the mean ± SD. ***p < 0.001, unpaired t test.

(D) ALDOA levels (Probe: Hs6-28-17-24) in patients with primary (n = 32) and metastatic prostate cancer (n = 20) in GSE6099. Data represent the mean ± SD. **p < 0.01, unpaired t test.

(E) ALDOA levels (Probe: A_23_P88963 and A_24_P921584) in patients with primary (n = 22), bone metastatic (n = 20), and liver metastatic prostate cancer (n = 21) in GSE77930. Data represent the mean ± SD. *p < 0.05, ***p< 0.001, unpaired t test.

(F–I) Receiver operating characteristic plots of ALDOA in patients with prostate cancer with or without metastasis from GSE3325 (F), GSE6919 (G), GSE6099 (H) and GSE77930 (I). Patients with bone metastatic and liver metastatic prostate cancer were combined as metastatic prostate cancer for GSE77930 in (I)

(J) Kaplan-Meier analysis (GEPIA 2) of disease-free survival in prostate cancer (n = 492).

to our understanding of metastatic disease and stands to provide impactful therapeutic targets of increased pertinence to the clinical management of advanced patients.

In the present work, we used a library-screening approach to identify cancer cell intrinsic factors that facilitate macrometastasis generation in the mouse lung as an experimental secondary tissue. This library platform has been previously leveraged in *in vitro* screens aimed at identifying regulators of a variety of biological processes ranging from bacterial (Bradley et al., 2001) or viral (Stremlau et al., 2004) infections to cancer cell death (Martin et al., 2004; Yamaji et al., 2010) or senescence (Brummelkamp et al., 2002). Here, this methodology has been used *in vivo*, identifying a critical role for ALDOA as a promalignant factor that

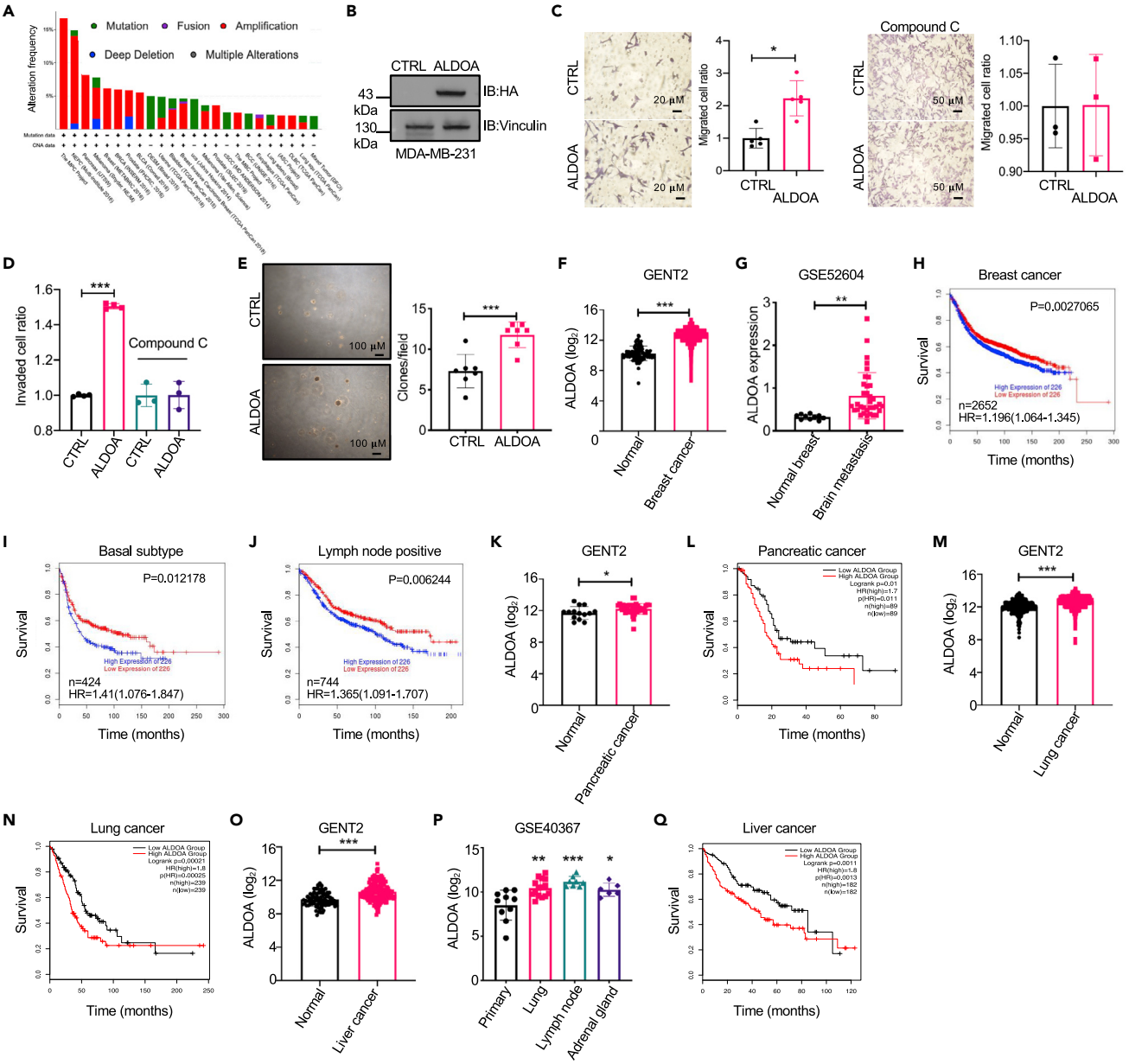

Figure 4. ALDOA is a poor prognosis cancer biomarker

(A) The mutation and copy number status of ALDOA in curated sets of nonredundant studies (TCGA, n = 44,347).

(B) Representative of n > 3 Western blots on lysates of MDA-MB-231 cells stably overexpressing HA-ALDOA. Vinculin was used as a loading control.

(C) Left: representative images and quantification of migration analyses of control versus HA-ALDOA-overexpressing MDA-MB-231 cells. Data are displayed as mean ± SD of n = 5 in triplicates each. Right: representative images and quantification of migration analyses of control versus HA-ALDOA-overexpressing MDA-MB-231 cells (we used $75X10^3$ cells/well in these experiments instead of $25X10^3$ cells) treated with Compound C (5 μM). Data are displayed as mean ± SD of n = 3 in triplicates each. *p < 0.05, unpaired t test. Scale bars indicate 20 μm or 50 μm as shown.

(D) Quantification of invasion analyses of control versus HA-ALDOA-overexpressing MDA-MB-231 cells with (n = 4) or without treatment of Compound C (5 μM) (n = 3). ***p < 0.001, unpaired t test. Scale bars indicate 100 μm.

(E) Representative images (left) and quantification (right) of soft-agar analyses of control versus HA-ALDOA-overexpressing MDA-MB-231 cells. Data are displayed as mean ± SD of n = 7 in triplicates each. ***p < 0.001, unpaired t test.

(F) ALDOA levels in normal patients (n = 93) and patients with breast cancer (n = 4293) from GENT2. Data represent the mean ± SD. ***p < 0.001, unpaired t test.

(G) ALDOA levels (Probe: A_23_P88963) in patients with primary (n = 10) and brain metastatic breast cancer (n = 35) in GSE52604. Data represent the mean ± SD. **p < 0.01, unpaired t test.

Figure 4. *Continued*

(H–J) Kaplan-Meier analysis (MTCI) of ALDOA (Gene ID:226) in breast cancer (n = 2652) (H), basal breast cancer (n = 424) (I) and lymph node positive breast cancer (n = 744) (J).

(K) ALDOA levels in normal patients (n = 14) and patients with pancreatic cancer (n = 41) from GENT2. Data represent the mean ± SD. *p < 0.05, unpaired t test.

(L) Kaplan-Meier analysis (GEPIA 2) of ALDOA in patients with pancreatic cancer (n = 178).

(M) ALDOA levels in normal patients (n = 499) and patients with lung cancer (n = 1117) from GENT2. Data represent the mean ± SD. ***p < 0.001, unpaired t test.

(N) Kaplan-Meier analysis (GEPIA 2) of ALDOA in lung cancer (n = 478).

(O) ALDOA levels in normal patients (n = 82) and patients with liver cancer (n = 174) from GENT2. Data represent the mean ± SD. ***p < 0.001, unpaired t test.

(P) ALDOA levels (Probe: 200966_x_at and 214687_x_at) in patients with primary hepatocellular carcinoma (n = 10) or in lung (n = 15), lymph node (n = 8), or adrenal gland (n = 6) metastasis in GSE40367. Data represent the mean ± SD. *p < 0.05, **p < 0.01, ***p < 0.001, ANOVA with Dunnett's test. Each group compared with the primary group.

(Q): Kaplan-Meier analysis (GEPIA 2) of ALDOA in liver cancer (n = 364).

experimentally promoted prostate cancer cell motility, anchorage-independent growth, and metastatic colonization and which tightly associated with disease progression and patient outcome, not only in prostate cancer patients but also in breast, liver, pancreatic, and lung cancer cohorts as well. Although our experimental findings have cast a role for ALDOA in macrometastasis formation specifically, they were in keeping with previously described associations of ALDOA with tumorigenesis and tumor progression in osteosarcoma (Chen et al., 2014), colorectal cancer (Kawai et al., 2017; Ye et al., 2018), oral squamous-cell carcinoma (Lessa et al., 2013), lung adenocarcinoma (Lin et al., 2011), lung squamous-cell carcinoma (Du et al., 2014), or clear-cell renal-cell carcinoma (Na et al., 2017). Altogether, these results were highly suggestive of widespread supportive roles of ALDOA in human tumor pathogenesis in general.

We found that ALDOA promoted the phosphoactivation of AMPK, which we showed was essential for ALDOA-regulated malignant traits, such as increased migration/invasion and anchorage-independent growth, two critical contributors to metastatic colonization. AMPK itself is a nutrient sensor that plays important regulatory roles in energy homeostasis and metabolic reprogramming under stress, and it has been described to control a plethora of traits that contribute to metastasis (Faubert et al., 2015; Liang and Mills, 2013; Steinberg and Carling, 2019). In prostate cancer cells specifically and in line with our observations, AMPK mediated the promigratory activities of microenvironmental adiponectin (Tang and Lu, 2009). Similarly, AMPK was critical to the functions of the cell-migration-inducing protein (CEMIP), found elevated in anoikis-resistant prostate cancer cells, initiating a GSK-3β/β-catenin/PDK4 pathway that additionally reprogrammed the metabolic landscape of migrating cancer cells (Zhang et al., 2018). In these respects, AMPK-induced reprogramming, which essentially promoted the adaptation of prostate cancer cells to survive environmental challenges, can also foster chemotherapy resistance via initiating autophagy (Lin et al., 2020). Of relevance, functions of AMPK in supporting the survival of DTCs under duress have also been observed in several other tumor types, including breast, lung, and blood cancers, to name a few (Avivar-Valderas et al., 2013; Jeon et al., 2012; Jin et al., 2018; Kishton et al., 2016; Li et al., 2020; Saito et al., 2015). We posit that AMPK operates within these capacities in our model as metastasizing disseminated cancer cells overcome intrinsic and extrinsic constraints to form macrocolonies in secondary tissues.

AMPK is activated allosterically by AMP, which together with ADP preserves the phosphorylation of Thr172, a hallmark of AMPK activation (Steinberg and Carling, 2019). Conversely, ATP counterbalances the actions of AMP and ADP, rendering AMPK activation primarily dependent on elevated ratios of AMP/ATP and to a much lesser extent, ratios of ADP/ATP (Lin and Hardie, 2018). In addition, AMP promotes AMPK activation by enhancing the formation of a ternary complex between AXIN, AMPK, and LKB1 in which the latter phosphorylates AMPK on Thr172 (Zhang et al., 2013). When translocated to the surface of the lysosome, AXIN and LKB1 associate with and form a complex with vacuolar ATPase and Ragulator, again leading to recruitment and phosphoactivation of AMPK (Zhang et al., 2014), but this time, in an adenine-nucleotide-independent manner. The rise in AMP levels and of the AMP/ATP ratio, increased by 49% and 36%, respectively, in HA-ALDOA-expressing cells compared with controls (Figures S4A and S5), would certainly be consistent with the nucleotide-dependent canonical AMPK activation by ALDOA. However, it is equally possible for ALDOA-induced AMPK activation to operate via AMP-independent mechanisms in our metastatic cells, such as via direct actions of FBP. Indeed, ALDOA interacts with v-ATPase (Kane, 2012) and directly regulates/activates the AXIN:Ragulator:LKB1:AMPK complex (Zhang et al., 2017). Here, FBP has been shown

to act as an inhibitor of ALDOA binding to and activation of this lysosomal complex (Zhang et al., 2017), and it was shown that even a small drop in FBP concentration in cells (comparable to the one we see as a result of ALDOA expression in our cells; see Figure S4B) was able to cause ALDOA coupling to the AMPK complex, resulting in its activation (Lin and Hardie, 2018). Of note, however, is that the latter model has been established in normal cells placed in metabolic stress, and it remains to be verified in cancer cells tested under similar conditions.

In summary, our research identified roles for an ALDOA-AMPK pathway in tumor progression, and provided the proof of principle for an *in vivo* GOF retroviral library screening approach that has proven useful in the identification of a genetic driver of tumor colonization. Although we have only validated ALDOA here, other recovered genes, such as RPSA, described to be involved in regulating cellular invasion (Wu et al., 2019), or CLN8, reported to be critical for lysosome biogenesis (di Ronza et al., 2018), a key process in tumor progression (Hamalisto and Jaattela, 2016), would certainly deserve further investigations in the context of metastatic colonization.

Limitations of the study

Our study has two main limitations. First, although we clearly showed in our models that ALDOA caused AMPK activation, the precise molecular mechanisms underlying such activation remain to be identified. Second, we showed that AMPK activity was needed for ALDOA promalignant activities, such as migration, invasion, and anchorage-independent growth, but detailed contributions of AMPK to micro-to-macro colony transition using *in vivo* models remain to be more fully characterized.

Resource availability

Lead contact

Further information and requests for resources and reagents should be directed to and will be fulfilled by the lead contact: Dr. Antoine E. Karnoub, Email: akarnoub@bidmc.harvard.edu; Phone: (617) 735–2082.

Materials availability

Cell lines and constructs generated in this study will be available upon request.

Data and code availability

This study did not generate any custom code, software, or algorithm.

METHODS

All methods can be found in the accompanying transparent methods supplemental file.

SUPPLEMENTAL INFORMATION

Supplemental information can be found online at https://doi.org/10.1016/j.isci.2021.102425.

ACKNOWLEDGMENTS

We thank A. Contreras, R. Awwad, B. Cuiffo, and J. Konge for technical help. We acknowledge institutional support from Beth Israel Deaconess Medical Center (to AEK), NCI grants R37 CA251543 and K08 CA201483 (to AMI), Department of Defense BCRP grants BC160702 and BC142139 (to AEK), and NCI grant CA207322 (to AEK).

AUTHOR CONTRIBUTIONS

ZT, YZ, MA, and TO collected and analyzed molecular, cellular, and animal data. SH conducted and analyzed Mass Spectrometry data with supervision and guidance of AMI. ZT and AEK wrote the manuscript with input from all co-authors. AEK designed and supervised overall research.

DECLARATION OF INTERESTS

The authors declare no competing interests.

Received: October 5, 2020
Revised: February 22, 2021
Accepted: April 9, 2021
Published: May 21, 2021

REFERENCES

Avivar-Valderas, A., Bobrovnikova-Marjon, E., Alan Diehl, J., Bardeesy, N., Debnath, J., and Aguirre-Ghiso, J.A. (2013). Regulation of autophagy during ECM detachment is linked to a selective inhibition of mTORC1 by PERK. Oncogene *32*, 4932–4940.

Berns, K., Hijmans, E.M., Koh, E., Daley, G.Q., and Bernards, R. (2000). A genetic screen to identify genes that rescue the slow growth phenotype of c-myc null fibroblasts. Oncogene *19*, 3330–3334.

Bradley, K.A., Mogridge, J., Mourez, M., Collier, R.J., and Young, J.A. (2001). Identification of the cellular receptor for anthrax toxin. Nature *414*, 225–229.

Brummelkamp, T.R., Kortlever, R.M., Lingbeek, M., Trettel, F., MacDonald, M.E., van Lohuizen, M., and Bernards, R. (2002). TBX-3, the gene mutated in Ulnar-Mammary Syndrome, is a negative regulator of p19ARF and inhibits senescence. J. Biol. Chem. *277*, 6567–6572.

Chen, X., Yang, T.T., Zhou, Y., Wang, W., Qiu, X.C., Gao, J., Li, C.X., Long, H., Ma, B.A., Ma, Q., et al. (2014). Proteomic profiling of osteosarcoma cells identifies ALDOA and SULT1A3 as negative survival markers of human osteosarcoma. Mol. Carcinog. *53*, 138–144.

di Ronza, A., Bajaj, L., Sharma, J., Sanagasetti, D., Lotfi, P., Adamski, C.J., Collette, J., Palmieri, M., Amawi, A., Popp, L., et al. (2018). CLN8 is an endoplasmic reticulum cargo receptor that regulates lysosome biogenesis. Nat. Cell Biol. *20*, 1370–1377.

DiNatale, A., and Fatatis, A. (2019). The bone microenvironment in prostate cancer metastasis. Adv. Exp. Med. Biol. *1210*, 171–184.

Du, S., Guan, Z., Hao, L., Song, Y., Wang, L., Gong, L., Liu, L., Qi, X., Hou, Z., and Shao, S. (2014). Fructose-bisphosphate aldolase a is a potential metastasis-associated marker of lung squamous cell carcinoma and promotes lung cell tumorigenesis and migration. PLoS One *9*, e85804.

Faubert, B., Vincent, E.E., Poffenberger, M.C., and Jones, R.G. (2015). The AMP-activated protein kinase (AMPK) and cancer: many faces of a metabolic regulator. Cancer Lett. *356*, 165–170.

Fulop, T., and Larbi, A. (2002). Putative role of 67 kDa elastin-laminin receptor in tumor invasion. Semin. Cancer Biol. *12*, 219–229.

Garcia, D., and Shaw, R.J. (2017). AMPK: mechanisms of cellular energy sensing and restoration of metabolic balance. Mol. Cell *66*, 789–800.

Giancotti, F.G. (2013). Mechanisms governing metastatic dormancy and reactivation. Cell *155*, 750–764.

Hamalisto, S., and Jaattela, M. (2016). Lysosomes in cancer-living on the edge (of the cell). Curr. Opin. Cell Biol. *39*, 69–76.

He, L., Ingram, A., Rybak, A.P., and Tang, D. (2010). Shank-interacting protein-like 1 promotes tumorigenesis via PTEN inhibition in human tumor cells. J. Clin. Invest. *120*, 2094–2108.

Jeon, S.M., Chandel, N.S., and Hay, N. (2012). AMPK regulates NADPH homeostasis to promote tumour cell survival during energy stress. Nature *485*, 661–665.

Jin, L., Chun, J., Pan, C., Kumar, A., Zhang, G., Ha, Y., Li, D., Alesi, G.N., Kang, Y., Zhou, L., et al. (2018). The PLAG1-GDH1 Axis promotes anoikis resistance and tumor metastasis through CamKK2-AMPK signaling in LKB1-deficient lung cancer. Mol. Cell *69*, 87–99 e87.

Kane, P.M. (2012). Targeting reversible disassembly as a mechanism of controlling V-ATPase activity. Curr. Protein Pept. Sci. *13*, 117–123.

Kawai, K., Uemura, M., Munakata, K., Takahashi, H., Haraguchi, N., Nishimura, J., Hata, T., Matsuda, C., Ikenaga, M., Murata, K., et al. (2017). Fructose-bisphosphate aldolase A is a key regulator of hypoxic adaptation in colorectal cancer cells and involved in treatment resistance and poor prognosis. Int. J. Oncol. *50*, 525–534.

Kienast, Y., von Baumgarten, L., Fuhrmann, M., Klinkert, W.E., Goldbrunner, R., Herms, J., and Winkler, F. (2010). Real-time imaging reveals the single steps of brain metastasis formation. Nat. Med. *16*, 116–122.

Kishton, R.J., Barnes, C.E., Nichols, A.G., Cohen, S., Gerriets, V.A., Siska, P.J., Macintyre, A.N., Goraksha-Hicks, P., de Cubas, A.A., Liu, T., et al. (2016). AMPK is essential to balance glycolysis and mitochondrial metabolism to control T-ALL cell stress and survival. Cell Metab. *23*, 649–662.

Lessa, R.C., Campos, A.H., Freitas, C.E., Silva, F.R., Kowalski, L.P., Carvalho, A.L., and Vettore, A.L. (2013). Identification of upregulated genes in oral squamous cell carcinomas. Head Neck *35*, 1475–1481.

Li, Y., Liang, R., Sun, M., Li, Z., Sheng, H., Wang, J., Xu, P., Liu, S., Yang, W., Lu, B., et al. (2020). AMPK-dependent phosphorylation of HDAC8 triggers PGM1 expression to promote lung cancer cell survival under glucose starvation. Cancer Lett. *478*, 82–92.

Liang, J., and Mills, G.B. (2013). AMPK: a contextual oncogene or tumor suppressor? Cancer Res. *73*, 2929–2935.

Lin, C.C., Chen, L.C., Tseng, V.S., Yan, J.J., Lai, W.W., Su, W.P., Lin, C.H., Huang, C.Y., and Su, W.C. (2011). Malignant pleural effusion cells show aberrant glucose metabolism gene expression. Eur. Respir. J. *37*, 1453–1465.

Lin, J.Z., Wang, W.W., Hu, T.T., Zhu, G.Y., Li, L.N., Zhang, C.Y., Xu, Z., Yu, H.B., Wu, H.F., and Zhu, J.G. (2020). FOXM1 contributes to docetaxel resistance in castration-resistant prostate cancer by inducing AMPK/mTOR-mediated autophagy. Cancer Lett. *469*, 481–489.

Lin, S.C., and Hardie, D.G. (2018). AMPK: sensing glucose as well as cellular energy status. Cell Metab. *27*, 299–313.

Long, F., Cai, X., Luo, W., Chen, L., and Li, K. (2014). Role of aldolase A in osteosarcoma progression and metastasis: in vitro and in vivo evidence. Oncol. Rep. *32*, 2031–2037.

Martin, S.S., Ridgeway, A.G., Pinkas, J., Lu, Y., Reginato, M.J., Koh, E.Y., Michelman, M., Daley, G.Q., Brugge, J.S., and Leder, P. (2004). A cytoskeleton-based functional genetic screen identifies Bcl-xL as an enhancer of metastasis, but not primary tumor growth. Oncogene *23*, 4641–4645.

Morisaki, T., Yashiro, M., Kakehashi, A., Inagaki, A., Kinoshita, H., Fukuoka, T., Kasashima, H., Masuda, G., Sakurai, K., Kubo, N., et al. (2014). Comparative proteomics analysis of gastric cancer stem cells. PLoS One *9*, e110736.

Na, N., Li, H., Xu, C., Miao, B., Hong, L., Huang, Z., and Jiang, Q. (2017). High expression of Aldolase A predicts poor survival in patients with clear-cell renal cell carcinoma. Ther. Clin. Risk Manag. *13*, 279–285.

Obenauf, A.C., and Massague, J. (2015). Surviving at a distance: organ-specific metastasis. Trends Cancer *1*, 76–91.

Saito, Y., Chapple, R.H., Lin, A., Kitano, A., and Nakada, D. (2015). AMPK protects leukemia-initiating cells in myeloid leukemias from metabolic stress in the bone marrow. Cell Stem Cell *17*, 585–596.

Siegel, R.L., Miller, K.D., and Jemal, A. (2020). Cancer statistics, 2020. CA Cancer J. Clin. *70*, 7–30.

Spano, D., Heck, C., De Antonellis, P., Christofori, G., and Zollo, M. (2012). Molecular networks that regulate cancer metastasis. Semin. Cancer Biol. *22*, 234–249.

Steeg, P.S. (2016). Targeting metastasis. Nat. Rev. Cancer *16*, 201–218.

Steinberg, G.R., and Carling, D. (2019). AMP-activated protein kinase: the current landscape for drug development. Nat. Rev. Drug Discov. *18*, 527–551.

Stremlau, M., Owens, C.M., Perron, M.J., Kiessling, M., Autissier, P., and Sodroski, J. (2004). The cytoplasmic body component TRIM5alpha restricts HIV-1 infection in Old World monkeys. Nature *427*, 848–853.

Tang, C.H., and Lu, M.E. (2009). Adiponectin increases motility of human prostate cancer cells via adipoR, p38, AMPK, and NF-kappaB pathways. Prostate *69*, 1781–1789.

Vanharanta, S., and Massague, J. (2013). Origins of metastatic traits. Cancer Cell *24*, 410–421.

Wu, Y., Tan, X., Liu, P., Yang, Y., Huang, Y., Liu, X., Meng, X., Yu, B., Wu, M., and Jin, H. (2019). ITGA6 and RPSA synergistically promote pancreatic cancer invasion and metastasis via PI3K and MAPK signaling pathways. Exp. Cell Res. *379*, 30–47.

Yamaji, T., Nishikawa, K., and Hanada, K. (2010). Transmembrane BAX inhibitor motif containing (TMBIM) family proteins perturbs a trans-Golgi network enzyme, Gb3 synthase, and reduces Gb3 biosynthesis. J. Biol. Chem. *285*, 35505–35518.

Ye, F., Chen, Y., Xia, L., Lian, J., and Yang, S. (2018). Aldolase A overexpression is associated with poor prognosis and promotes tumor progression by the epithelial-mesenchymal transition in colon cancer. Biochem. Biophys. Res. Commun. *497*, 639–645.

Zhang, C.S., Hawley, S.A., Zong, Y., Li, M., Wang, Z., Gray, A., Ma, T., Cui, J., Feng, J.W., Zhu, M., et al. (2017). Fructose-1,6-bisphosphate and aldolase mediate glucose sensing by AMPK. Nature *548*, 112–116.

Zhang, C.S., Jiang, B., Li, M., Zhu, M., Peng, Y., Zhang, Y.L., Wu, Y.Q., Li, T.Y., Liang, Y., Lu, Z., et al. (2014). The lysosomal v-ATPase-Ragulator complex is a common activator for AMPK and mTORC1, acting as a switch between catabolism and anabolism. Cell Metab. *20*, 526–540.

Zhang, P., Song, Y., Sun, Y., Li, X., Chen, L., Yang, L., and Xing, Y. (2018). AMPK/GSK3beta/beta-catenin cascade-triggered overexpression of CEMIP promotes migration and invasion in anoikis-resistant prostate cancer cells by enhancing metabolic reprogramming. FASEB J. *32*, 3924–3935.

Zhang, P., Zhai, Y., Cai, Y., Zhao, Y., and Li, Y. (2019). Nanomedicine-based immunotherapy for the treatment of cancer metastasis. Adv. Mater. *31*, e1904156.

Zhang, Y.L., Guo, H., Zhang, C.S., Lin, S.Y., Yin, Z., Peng, Y., Luo, H., Shi, Y., Lian, G., Zhang, C., et al. (2013). AMP as a low-energy charge signal autonomously initiates assembly of AXIN-AMPK-LKB1 complex for AMPK activation. Cell Metab. *18*, 546–555.

iScience, Volume *24*

Supplemental information

In vivo library screening identifies the metabolic enzyme aldolase A as a promoter of metastatic lung colonization

Zhenbo Tu, Shengqi Hou, Yurong Zheng, Maerjianghan Abuduli, Tamer Onder, Andrew M. Intlekofer, and Antoine E. Karnoub

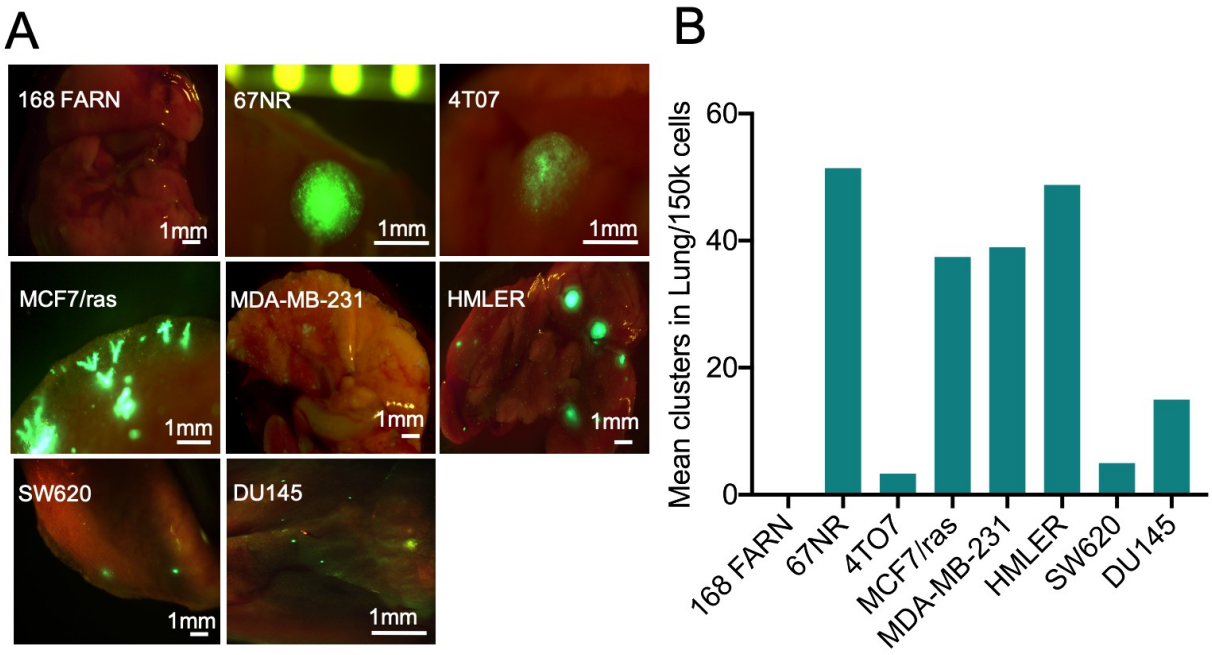

Supplementary Figure 1. ***Screen of the metastatic colonization propensity of GFP-labeled cancer cells in mouse lungs****, Related to Fig. 1.*
(A) Representative images of GFP-fluorescence in mouse lungs after introduction of the indicated cells ($150x10^3$) into circulation with n=7-10 mice per cell line. Scale bars indicate 1mm.
(B) Quantification of microscopic metastases in A.

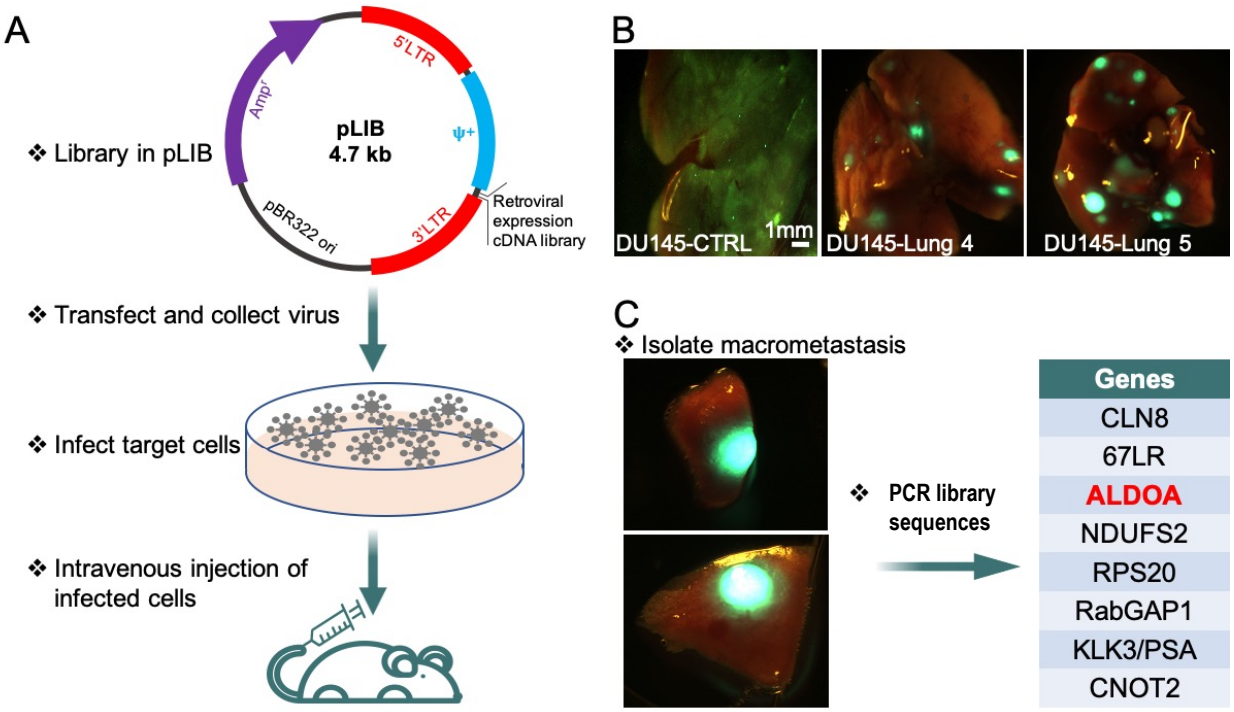

Supplementary Figure 2. ***In vivo cDNA library screen for cancer cell metastatic colonization****, Related to Fig. 1.*
(A) Schematic representation of the library screening approach.
(B) Representative fluorescence pictures of lungs isolated from mice injected 18 days earlier with GFP-DU145 cells ($150x10^3$) infected with control or human prostate pLIB-cDNA library (CTRL and Lung 4/5, respectively). Scale bar indicates 1mm.
(C) Macrocolonies were surgically isolated from whole lungs and their genomic DNA was harvested. Inserted library sequences were then amplified by PCR and products were sequenced. Recovered full sequences included the listed genes.

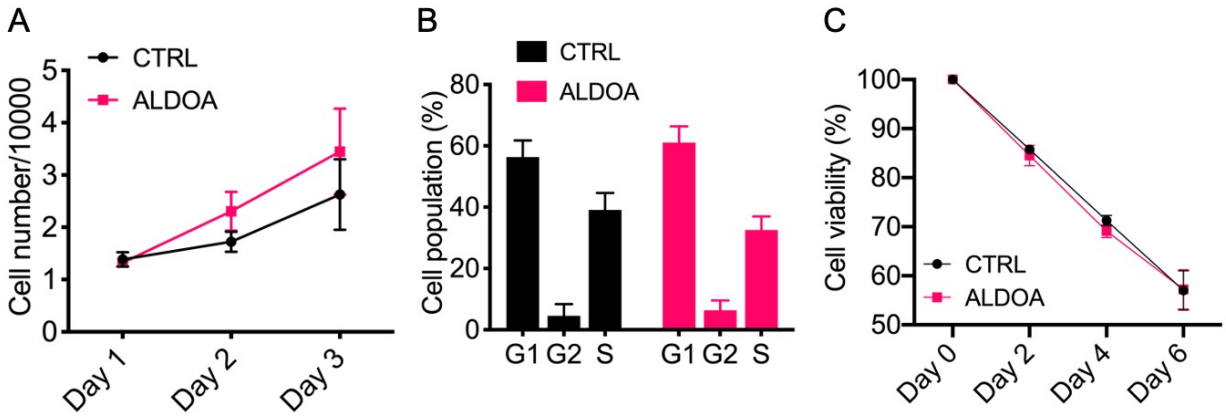

Supplementary Figure 3. ***ALDOA does not impact proliferation or resistance to matrix deprivation****, Related to Fig. 1.*

(A) Cell growth of control or HA-ALDOA-expressing DU145 cells estimated by Trypan blue exclusion assay on the indicated days (n>3 in triplicates each). Data represent the mean ± SD.

(B) Cell cycle quantification in control or HA-ALDOA-expressing DU145 cells (n>3 in triplicates each) estimated by FACS-based analyses. Data represent the mean ± SD.

(C) Cell viability of suspended control and HA-ALDOA-expressing DU145 cells estimated using Trypan blue exclusion assay on the indicated days (n>3 in triplicates each). Data represent the mean ± SD.

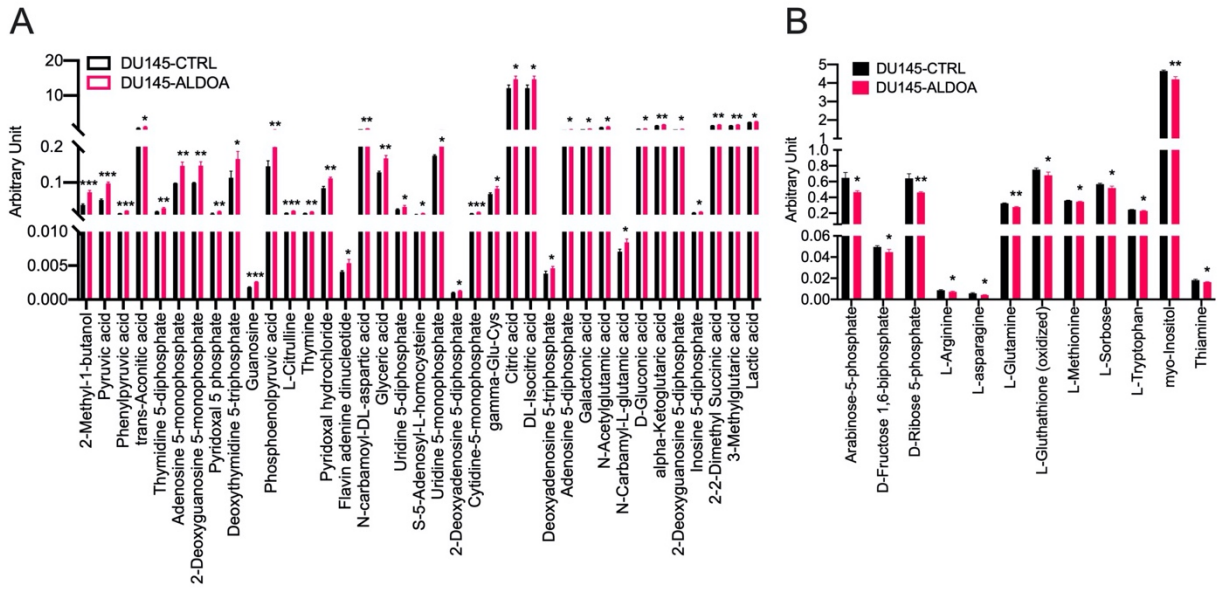

Supplementary Figure 4. ***LC/MS-based metabolic analyses****, Related to Fig. 2.*
(A-B) LC/MS-based metabolic profiling showing significant upregulations of metabolites associated with HA-ALDOA-overexpression. Of a total of ~122 products, 37 were significantly upregulated (A) and 12 were significantly downregulated (B) based on MetaboAnalyst algorithm using LC/MS analysis between DU145 cells stably expressing HA-ALDOA and controls as input. Data represent the mean ± SD of n=3 experiments performed in triplicates. * p<0.05, **<0.001,***p<0.0001, unpaired t test.

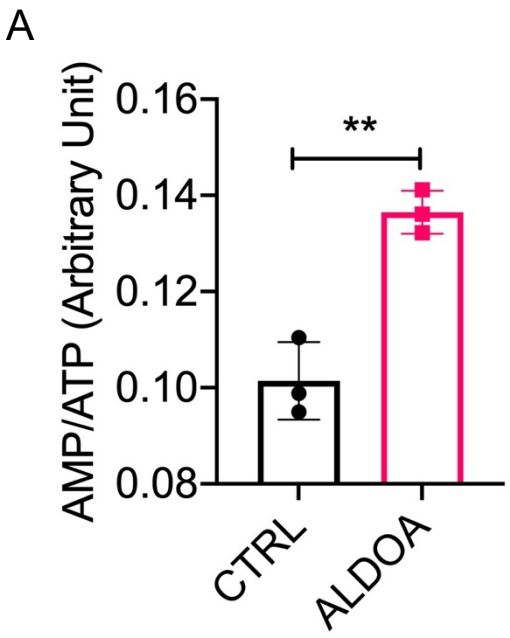

Supplementary Figure 5. ***The AMP/ATP ratio in LC/MS-based metabolic profiling****, Related to Fig. 2.*

(A) The AMP over ATP ratio was derived from Adenosine 5-monophosphate and adenosine 5-triphosphate levels determined using LC/MS metabolic profiling in Figure S4. Data represent the mean ± SD. **p < 0.01, unpaired t test.

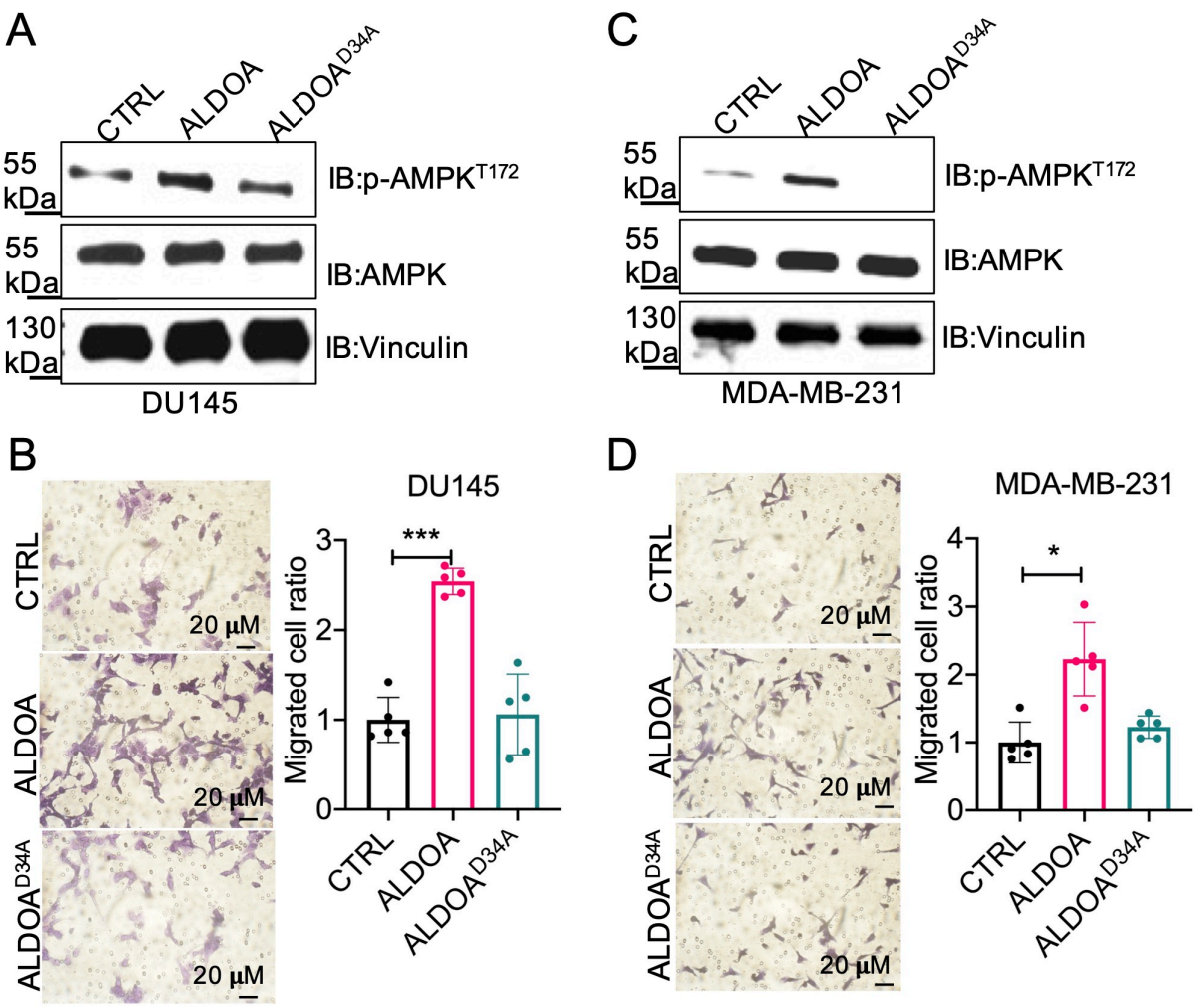

Supplementary Figure 6. ***Enzymatically inactive HA-ALDOA is unable to promote AMPK phosphorylation and cancer cell migration***, *Related to Fig. 2.*

(A) Representative (n>3) Western blots of phospho-AMPK and AMPK in DU145 cells stably expressing HA-ALDOA, HA-ALDOA^{D34A} and controls.

(B) Representative images (left) and quantification (right) of migration analyses of control versus HA-ALDOA and HA-ALDOA^{D34A}-overexpressing DU145 cells. Data are displayed as mean ± SD of n=5 in triplicates each. ***p < 0.001, unpaired t test. ANOVA with Dunnett's test was used. Each group compared to CTRL group.

(C) Representative (n>3) Western blots of phospho-AMPK and AMPK in MDA-MB-231 cells stably expressing HA-ALDOA, HA-ALDOA^{D34A} and controls.

(D) Representative images (left) and quantification (right) of migration analyses of control versus HA-ALDOA and HA-ALDOA^{D34A}-overexpressing MDA-MB-231 cells. Data are displayed as mean ± SD of n=5 in triplicates each. *p < 0.05, unpaired t test. ANOVA with Dunnett's test was used. Each group was compared to CTRL group. For B and D, scale bars indicate 20 μm.

Antibody	Source	Catalog#	RRID	Assay(s)
Rabbit anti-β-actin (13E5)	CST	4970	AB_2223172	WB
Rabbit anti-AMPKα1	CST	2795	AB_560856	WB
Rabbit anti-AMPK-α, phospho (Thr172) (40H9)	CST	2535	AB_331250	WB
Rabbit anti-GAPDH (14C10)	CST	2118	AB_561053	WB
Rabbit anti-Vinculin	CST	4650	AB_10559207	WB
Mouse anti-HA (12CA5)	Roche	11666606001	AB_514506	WB

Supplementary Table 1. ***Antibodies Used.*** *Related to Figs 1, 2, 4 and Supplementary Fig. 6.*

TRANSPARENT METHODS

All experiments described herein were conducted with the regulatory approval of the Harvard Committee on Microbiological Safety (COMS) and the Institutional Animal Care and Use Committee (IACUC).

Cell cultures

Mouse mammary carcinoma cell lines 67NR, 4T07, and 168 FARN, human mammary cancer cells HMLER and MCF7 cells expressing HRasV12 (MCF7/Ras), and human male colon cancer cells SW620 were obtained from Dr. Robert Weinberg (Whitehead Institute for Biomedical Research, Cambridge, MA). 67NR, 4T07, 168 FARN, and MCF7/Ras cells were grown in DMEM media (Cellgro, Corning, Tewksbury, MA) supplemented with 10% fetal bovine serum (FBS; Gibco BRL, Waltham, MA). HMLER were propagated in DMEM/F12 medium (Wisent Bioproducts, Saint-Jean Baptiste, QC) supplemented with 5% horse serum (Gibco BRL, Waltham, MA), insulin (10 µg/ml; Wisent Bioproducts, Saint-Jean Baptiste, QC), hydrocortisone (500 ng/ml; Sigma-Aldrich, St. Louis, MO), epidermal growth factor (20 ng/ml; R&D, Minneapolis, MN), and cholera toxin (100 ng/ml; List Biological Laboratories, Campbell, CA). Human mammary MDA-MB-231 and prostate PC3 and DU145 cancer cells were purchased from American Type Culture Collection (ATCC, Atlanta, GA) and grown in DMEM media (Cellgro, Corning, Tewksbury, MA) supplemented with 10% fetal bovine serum (FBS; Gibco BRL, Waltham, MA). Human prostate cancer cells LNCAP, C4-2 and RV-1 were a generous gift from Dr. Steven Balk (Beth Israel Deaconess Medical Center, Boston, MA) and were grown in RPMI 1640 media (Cellgro, Corning, Tewksbury, MA) supplemented with 10% FBS (Gibco BRL, Waltham, MA).

Viral transductions

HEK293T cells were transfected with pRRL3-GFP (Cuiffo et al., 2014), pCMV-VSV-G (Addgene #8454), and pCMV-dR8.2 dvpr (Addgene #8455) plasmids using Fugene HD (Roche Applied Science, Indianapolis, IN) according to manufacturer's recommendations. At 48 hrs, viral particles were collected, passed through 0.45 µm-filters (Puradisc 25mm, Whatman), and transduced into recipient cells in the presence of 5 µg/ml polybrene (Americanbio Inc, Canton, MA). GFP-labeling of the cells was confirmed by fluorescence microscopy to be >99%.

For library transductions, retroviral cDNA derived from human prostate (containing $>8.0x10^6$ clones, with a cDNA size range of 0.5-5.0 kb and with average size cDNA length of 1.6 kb) was purchased from Clontech (#634204; Heidelberg, Germany), and transfected into HEK293T cells along with pCMV-VSV-G and pUMVC (Addgene #8449) using Lipofectamine 2000 (Invitrogen, Carlsbad, CA). Viruses were recovered after 42-48 hrs, filtered as above, diluted 1:10, and allowed to infect recipient GFP-DU145 cells for 18 hrs in the presence of 5 µg/ml polybrene. The MOI for infection was 0.2 determined using pLAPSN as a control.

For ALDOA overexpression, *ALDOA* tagged with Haemagglutinin (HA) on the NH_2-terminus was first generated by Polymerase Chain Reaction (PCR) using OmicsLink expression clone EX-C0193-M60 (GeneCopeia, Rockville, MD) as a template open reading frame (ORF). Primers used were: 5'-primer with a BamH1 restriction site

GTGGATCCCCACCATGTACCCATACGATGTTCCAGATTACGCTCCCTACCAATATC C) and 3'-primer with an EcoR1 restriction site GGGAATTCCTAATAGGCGTGGTTAGAGACGAAGAGGGACTCGCTGGCAGC, and the generated amplicon was subcloned into pBabe-Puro plasmid (Addgene plasmid #1764). To ensure more robust and widespread ALDOA expression in target cells, HA-ALDOA was digested out of pBabe using BamH1 and Sal1 restriction enzymes and cloned in place of GFP into pLenti-CMV-GFP-Puro vector (Addgene plasmid #17448) to generate pLenti-CMV-HA-ALDOA expression vector. ALDOA D34A site mutation plasmid was generated by QuickChange Site-Directed Mutagenesis Kit (200518, Agilent Technologies, Santa Clare, CA) using primers (Forward: 5'-CATCCTGGCTGCAGCTGAGTCCACTGGGA-3'; Reverse: 5'-TCCCAGTGGACTCAGCTGCAGCCAGGATG-3') based on pLenti-CMV-HA-ALDOA expression vector. HA-ALDOA-carrying lentiviral particles were generated as mentioned above, transduced into GFP-DU145 cells, and stable lines generated by Puromycin (1-2 µg/ml; Wisent Bioproducts, Saint-Jean Baptiste, QC) selection.

Lung colonization assays

Boluses of 100 µl (1.5 x 10^5 cells) of GFP-labeled cancer cells suspended in PBS supplemented with 1% FBS were intravenously injected via tail ven into recipient 8-10 weeks old NOD/SCID mice. Animals were euthanized 18 days later, lungs excised, and metastatic colonies examined using fluorescence microscopy (Zeiss, Axvio). Male mice were used for DU145 and SW620 cells, and female mice were used for all other lines.

Genomic and quantitative PCR determinations

Individual macrometastatic colonies were surgically excised from explanted mouse lungs, and genomic DNA was harvested using Qiagen DNeasy (Qiagen, Germantown, MD). To identify pLIB-library-inserted integrated sequences, DNA was amplified with PicoMaxx High Fidelity PCR System (Agilent Technologies, Santa Clara, CA) using manufacturer-supplied 5' and 3' linker primers, and products were resolved using electrophoresis. PCR fragments were extracted using QIAquick Gel Extraction Kit (Qiagen, Germantown, MD) and then sent out for Sanger sequencing for BLAST identification against human gene databases.

For quantitative PCR, total RNA was isolated using RNeasy (Qiagen, Hilden, Germany), reverse transcribed into cDNA by Qiagen RT kit, and qPCR performed using Qiagen SYBR Green kit according to manufacturer's instructions. Primers used were: 18S forward, 5'-GTAACCCGTTGAACCCCATT-3'; 18S reverse, 5'-CCATCCAATCGGTAGTAGCG-3'; ALDOA forward, 5'-CAAGCGAGCCCTGGCCAACA-3'; ALDOA reverse, 5'-AGCCTGACCGCTCGGAGTGT-3'; ALDOB forward, 5'-GCCGACCAGTGTCCATCCAGC-3'; ALDOB reverse, 5'-ACCAGTCCATTCTGCTGACAGATGC-3'; ALDOC forward, 5'-CGGATCAGAACCCGAGCTGTGC-3'; ALDOC reverse, 5'-ATGGTGACAGCTCCCTGTGCG. Evaluation of transcript abundance was performed according to the $2^{-\Delta\Delta CT}$ method.

Western blot analyses
Western blots were performed using standard techniques with antibodies from Cell Signaling Technology (CST; Danvers, MA) recognizing β-actin (#4970), p-AMPK (#2535), AMPK (#2795), GAPDH (#2118) and Vinculin (#4650), or from Sigma (Sigma-Aldrich, St. Louis, MO) recognizing Anti-HA (12CA5) (#11666606001) (See Table S1). Blots were developed using chemiluminescence (BioRad, Hercules, CA).

Aldolase enzyme activity assay
Aldolase activity was measured using a coupled enzymatic assay as previously described by Bergmeyer (1974) using SP-FDP01 assay (MilliporeSigma, St. Louis, MO). Briefly, snap-frozen cells were lysed in buffer containing 0.5% NP-40 in 100 mM Tris HCl Buffer, pH 7.4, and 10 µg cleared total protein was processed for enzyme activity measurements in 100 mM Tris HCl pH 7.4 enzyme reaction buffer containing F1,6-DP, β-NADH, and α-GDH/TPI. The rate of β-NADH consumption in triplicate samples per condition was followed at 340 nm absorbance using spectrophotometry for ~5 min at 25^0C. Purified rabbit Aldolase A obtained from MP Biomedicals (#159859, Solon, OH) was used as a positive control.

Proliferation, anoikis, migration, invasion, anchorage-independent growth, and cell cycle analyses
Cell proliferation was measured using Trypan blue exclusion assay on $10x10^3$ cells cultured in 6-well plates in DMEM/10%FBS for 3 days. For viability in suspension, $500x10^3$ DU145 cells were suspended in 1.5-ml eppendorf tubes filled with DMEM/0.1%FBS. Tubes were placed under continuous rotation/tumbling and Trypan-blue-negative cells counted daily for 3 days. For cell migration, $25x10^3$ cells were placed in the upper chamber of 8 µm Falcon transwell insert (Corning Life Sciences, Tewksbury, MA). After 24h, filters were recovered, fixed with 4% paraformaldehyde (PFA), and stained with 0.5% crystal violet. Migrated cells were counted in five randomly selected microscope fields. For cell invasion, $25x10^3$ cells were placed in the upper chamber of 8 µm Tumor Invasion System insert (REF 354165, Corning Life Sciences, Tewksbury, MA). After 20h, media was removed from apical chambers, and inserts transferred into secondary 24-well plates containing 4 µg/ml calcein AM in HBSS for 1 hour, and then fluorescence of invaded cells read at wavelengths of 494/517 nm.

For anchorage-independent growth assays, a total of $5x10^3$ cells were suspended in 0.7% top agarose solution, and were seeded in 6-well plates on top of a 0.8% base agar layer. Wells were fed once a week for 3~6 weeks. Growth colonies were counted following staining with 0.005% Crystal Violet overnight at room temperature. For cell cycle analyses, growing and <70% confluent cultures were suspended, fixed with PFA, and stained with 0.005% Triton X-100, 0.1 mg DNase-free PureLink RNase A (Invitrogen, Carlsbad, CA) and 10 µg Propidium Iodide (Sigma-Aldrich, St. Louis, MO) and analyzed by FACS.

Liquid Chromatography-tandem-Mass Spectrometry (LC/MS)
Equal numbers of controls and HA-ALDOA-overexpressing DU145 cells were allowed to grow in 6-well plates to non-confluent densities. Metabolism was quenched and

metabolites were extracted by aspiration of media followed by immediate addition of ice-cold 80:20 methanol:water solution containing 2 µmol/L deuterated 2-hydroxyglutarate (D-2-hydroxyglutaric2,3,3,4,4-d5 acid; deuterated-2HG) as an internal standard. After overnight incubation at -80°C, cell remnants were scraped and transferred along with the methanol:water mixture into 1.5 ml centrifuge tubes, vortexed, and centrifuged at 14,000 g for 20 min at 4°C for protein precipitation. A 900 µl portion of the supernatant was moved to a fresh tube and then dried in an evaporator (Genevac EZ-2 Elite) for 18h. Dried extracts were resuspended in 40 µL of 97:3 water:methanol containing 10 mM tributylamine and 15 mM acetic acid. Samples were vortexed, incubated on ice for 20 min, and clarified by centrifugation at 20,000 g for 20 min at 4°C. LC-MS analysis used a Zorbax RRHD Extend-C18 column (150 mm × 2.1 mm, 1.8 µm particle size, Agilent Technologies). Solvent A was 10 mM tributylamine and 15 mM acetic acid in 97:3 water:methanol, and solvent B was 10 mM tributylamine and 15 mM acetic acid in methanol, prepared according to the manufacturer's instructions (MassHunter Metabolomics dMRM Database and Method, Agilent Technologies). LC separation was coupled to a 6470 triple quadrupole mass spectrometer (Agilent Technologies), which was operated in dynamic MRM (dMRM) scan type and negative ionization mode.

Bioinformatic and metabolomic analyses

Analyses of ALDOA protein-protein interaction networks was performed using STRING (https://string-db.org/cgi/input.pl). DAVID 6.8 (https://david.ncifcrf.gov/tools.jsp) was used to identify gene enrichment amongst genes that exhibited positive correlation with ALDOA ($r>0.25$, $p<0.05$) in Metastatic Prostate Adenocarcinoma (SU2C/PCF Dream Team) and in Metastatic Prostate Cancer (SU2C/PCF Dream Team) (https://www.cbioportal.org/). MetaboAnalyst (https://www.metaboanalyst.ca/), a statistical, functional and integrative analysis of metabolomics data, was performed for visualization of metabolic enrichment based on up-regulated metabolic products in DU145 cells stably expressing ALDOA. The expression levels of ALDOA in normal, prostate cancer, breast cancer, liver cancer, and lung cancer from GPL96 (HG-U133A) were analyzed using GENT2 (http://gent2.appex.kr/gent2/). Gene Expression Omnibus (https://www.ncbi.nlm.nih.gov/geo/) was used to analyze ALDOA levels in prostate cancer, breast cancer, and hepatocellular cancer patients with primary and metastatic tumors.

For survival analyses, patients were partitioned into High and Low groups according to ALDOA expression levels (with Median adopted as a cutoff). Prostate adenocarcinoma (PRAD), lung adenocarcinoma (LUAD), and liver hepatocellular carcinoma (LIHC) were accordingly analyzed by GEPIA 2 (http://gepia2.cancer-pku.cn/#survival) and breast cancers were analyzed via MTCI (http://glados.ucd.ie/BreastMark/mRNA_default.html). A total of 44347 patients from 'Curated set of non-redundant studies' were used for exploring ALDOA mutation and copy number alterations (CNA) status in TCGA (https://www.cbioportal.org/).

Statistical analysis

Results were expressed as mean ± SD and data analyzed using an unpaired Student's t test. One-way analysis of variance (ANOVA) with Dunnett's test for multiple comparisons was performed by GraphPad 8. The log-rank test was used to analyze

data in survival experiments. The diagnostic value of ALDOA was assessed using receiver operating characteristic (ROC) curves and Area under the ROC Curve (AUC) by using SPSS version 23. For all analyses, *, **, and *** indicated $p < 0.05$, $p < 0.01$, and $p < 0.001$, respectively.